

# A Temporally-Aware Interpolation Network for Video Frame Inpainting

Ximeng Sun\*, Ryan Szeto\*, and Jason J. Corso

University of Michigan, Ann Arbor, USA  
{sunxm,szeto,r,jjcorso}@umich.edu

**Abstract.** We propose the first deep learning solution to video frame inpainting, a challenging instance of the general video inpainting problem with applications in video editing, manipulation, and forensics. Our task is less ambiguous than frame interpolation and video prediction because we have access to both the temporal context and a partial glimpse of the future, allowing us to better evaluate the quality of a model’s predictions objectively. We devise a pipeline composed of two modules: a bidirectional video prediction module, and a temporally-aware frame interpolation module. The prediction module makes two intermediate predictions of the missing frames, one conditioned on the preceding frames and the other conditioned on the following frames, using a shared convolutional LSTM-based encoder-decoder. The interpolation module blends the intermediate predictions to form the final result. Specifically, it utilizes time information and hidden activations from the video prediction module to resolve disagreements between the predictions. Our experiments demonstrate that our approach produces more accurate and qualitatively satisfying results than a state-of-the-art video prediction method and many strong frame inpainting baselines.

**Keywords:** Video frame inpainting, video inpainting, video prediction, video interpolation

## 1 Introduction

In this work, we explore the video frame inpainting problem, i.e. the task of reconstructing a missing sequence of frames given both a sequence of *preceding* frames and a sequence of *following* frames. For example, if we were given a clip of someone winding up a baseball pitch and a clip of that person after he/she has released the ball, we would predict the clip of that person performing the throwing action. Example applications include video post-processing (e.g. adding frames to under-sampled or corrupted videos), animation (e.g. generating intermediate frames given a set of key frames), and spoofing (e.g. removing an unwanted object from a shot by replacing the segment in which it appears).

Our video frame inpainting task is a challenging instance of general video inpainting because we aim to fill in whole, temporally-contiguous frames. Most

---

\* indicates equal contribution

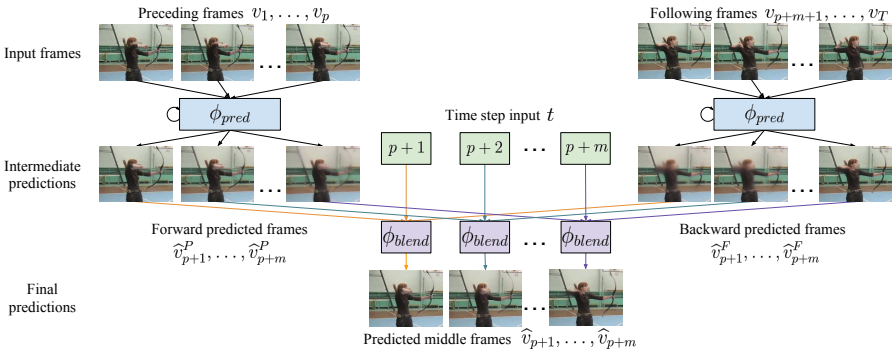


Fig. 1: Our high-level approach to video frame inpainting. We predict middle frames by blending forward and backward intermediate video predictions with a Temporally-Aware Interpolation (TAI) network

existing video inpainting methods assume that the “holes” in the video are localized to small spatio-temporal regions, and are thus not suited to tackle our task. Frame interpolation methods, which can only take in one frame before and one frame after the desired sequence, are also insufficient since their inputs do not capture the temporal context required to sufficiently constrain the solution. If we were given two images of a swinging pendulum, for instance, we could propose many plausible video clips, each depicting a period and offset of the pendulum that is consistent with the input. However, if we were given two *video clips*, only one period would be consistent with the depicted motion.

We present the first deep neural network for video frame inpainting, which approaches the problem in two steps as shown in Fig. 1. First, we use a video prediction subnetwork to generate two intermediate predictions of the middle frames: the “forward prediction” conditioned on the preceding frames, and the “backward prediction” conditioned on the following frames. Then, we blend each pair of corresponding frames together to obtain the final prediction.

Our blending strategy exploits three characteristics of our intermediate prediction process. First, a pair of corresponding intermediate predictions might be inconsistent, e.g. an actor might appear in two different locations. To address this, we introduce a blending neural network that can cleanly merge a given pair of predictions by reconciling the differences between them. Second, for any given time step, the forward and backward predictions are not equally reliable: the former is more accurate for earlier time steps, and the latter is more accurate for later time steps. Hence, we feed time step information directly into the blending network, making it *temporally-aware* by allowing it to blend differently depending on which time step it is operating at. Finally, the intermediate predictions come from a neural network whose hidden features may be useful for blending. To leverage these features, we feed them to the blending network as additional inputs. We call our blending module the **temporally-aware interpolation network** (or TAI network for short). As we show in our experiments, our approach yields the most visually satisfying predictions among several strong baselines and across multiple human action video datasets.

To summarize, we make three contributions. First, we propose a deep neural network that addresses the challenging video frame inpainting task by generating two intermediate predictions and blending them with our novel TAI network. Second, we propose and compare against several baselines that leverage the information provided by the preceding and following frames, but do not utilize our TAI blending approach. Finally, we demonstrate that our approach is quantitatively and qualitatively superior to the proposed baselines across three human action video datasets.

## 2 Related Work

Video frame inpainting is a challenging instance of the general video inpainting problem, which is itself the video equivalent of image inpainting [1,2,3,4,5,6,7,8,9]. In the general video inpainting problem, we are given a video that is missing arbitrary voxels (spatio-temporal pixels), and the goal is to fill each voxel with the correct value. Existing video inpainting methods typically fall into one of three categories: *patch-based* methods that search for complete spatio-temporal patches to copy into the missing area [10,11,12,13]; *object-based* methods that separate spatial content into layers (e.g. foreground and background), repair them individually, and stitch them back together [14,15]; and *probabilistic model-based* methods that assign values that maximize the likelihood under some probabilistic model [16,17,18]. Many of these approaches make strong assumptions about the video content, such as constrained camera pose/motion [12,14,15] or static backgrounds [14,15,17]. In addition, they usually do not assume that whole, contiguous frames are missing (i.e. the “holes” in the video are localized to small spatio-temporal regions), although a few methods have been evaluated in the more challenging setting [10,16]. Finally, to the best of our knowledge, no existing solution has leveraged deep neural networks, which can potentially outperform prior work thanks to the vast amounts of video data available online.

Our problem also shares many similarities to frame interpolation, the task of predicting one or more frames in between two (typically subsequent) input frames. While most classical approaches project a dense optical flow field to an arbitrary number of intermediate time steps [19,20,21], recent approaches train deep neural networks to learn the desired mapping from data [22,23,24,25]. However, all of these approaches require input frames that occur within a minuscule window of time (i.e. no more than 0.05 seconds apart). Furthermore, as explained in Sec. 1, individual frames lack the temporal context required to sufficiently constrain the desired solution.

Video prediction, where the goal is to generate the future frames that follow a given sequence of video frames, is yet another actively-studied area with an important limitation. The earliest approaches draw heavily from language modeling literature by extending simple recurrent sequence-to-sequence models to predict patches of video [26,27]; more recent methods utilize structured models that decompose the input data and/or the learned representations in order to facilitate training [28,29,30]. Unfortunately, the video prediction task is inherently

underconstrained since the past can diverge into multiple futures; consequently, plausible futures that deviate from the actual data are hard to evaluate.

In light of the limitations present in earlier work, video frame inpainting is an important task that deserves more attention. First, it is a very challenging instance of video inpainting in which whole, contiguous frames are missing; this challenge can be insurmountable for existing video inpainting methods that rely on the availability of local information. Second, it addresses the problems with frame interpolation by incorporating multiple frames that include temporal context and may lie several seconds apart. Finally, it addresses the inherent ambiguity of video prediction by providing a glimpse of the future as input, thereby constraining the content of the interpolated sequence and facilitating evaluation.

### 3 Approach

We define the video frame inpainting problem as follows. Let  $V = \{v_1, v_2, \dots, v_T\}$  be a sequence of frames from a real video,  $p$ ,  $m$ , and  $f$  be the number of “preceding”, “middle”, and “following” frames such that  $p + m + f = T$ , and  $P_V = \{v_1, \dots, v_p\}$ ,  $M_V = \{v_{p+1}, \dots, v_{p+m}\}$ ,  $F_V = \{v_{p+m+1}, \dots, v_T\}$  be the sequences of preceding, middle, and following frames from  $V$  respectively. We seek a function  $\phi$  that satisfies  $M_V = \phi(P_V, F_V)$  for all  $V$ .

We propose a novel neural network composed of two modules to approximate  $\phi$  (see Fig. 1). The first module  $\phi_{pred}$  (Sec. 3.2) is a video prediction network that produces a “forward prediction”  $\widehat{M}_V^P$  and a “backward prediction”  $\widehat{M}_V^F$  by conditioning on  $P_V$  and  $F_V$  respectively:

$$\widehat{M}_V^P = \phi_{pred}(P_V), \quad (1)$$

$$\widehat{M}_V^F = \phi_{pred}(F_V^R)^R, \quad (2)$$

where  $(\cdot)^R$  is an operation that reverses the input sequence. The second module  $\phi_{blend}$  (Sec. 3.1) takes corresponding pairs of frames from  $\widehat{M}_V^P$  and  $\widehat{M}_V^F$  that share the same time step, and blends them into the frames that makes up the final prediction  $\widehat{M}_V$ , i.e.

$$\widehat{M}_V = \phi_{blend}\left(\widehat{M}_V^P, \widehat{M}_V^F\right). \quad (3)$$

#### 3.1 Frame Blending Network $\phi_{blend}$

We start by motivating our Temporally-Aware Interpolation (TAI) network, the most novel technical contribution of our work. Suppose for each middle time step  $t \in \{p+1, \dots, p+m\}$ , we have a pair of corresponding frames from the forward and backward predictions  $(\widehat{v}_t^P, \widehat{v}_t^F)$ . Blending  $\widehat{v}_t^P$  and  $\widehat{v}_t^F$  is difficult because (i) they often contain mismatched content (e.g. between the pair of frames, an actor might be in different locations), and (ii) they are not equally reliable (e.g.  $\widehat{v}_t^P$  is more reliable for earlier time steps). Intuitively, equally averaging  $\widehat{v}_t^P$  and  $\widehat{v}_t^F$

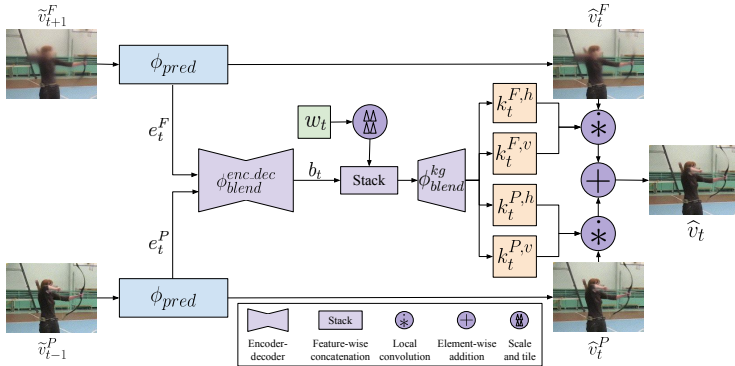


Fig. 2: The architecture of our TAI network

results in ghosting artifacts (e.g. multiple faded limbs in human action videos), but surprisingly, replacing a simple average with an off-the-shelf interpolation network shares the same problem, as we show in Sec. 4.5.

Our TAI network is an interpolation network that, aside from the pair of frames to blend, receives two additional types of information: the scaled time step to predict—defined as  $w_t = (t - p)/(m + 1)$ —and the intermediate activations from the bidirectional video prediction network  $e_t^P$  and  $e_t^F$ . We feed  $w_t$  to our interpolation network so it can learn how to incorporate the unequal reliability of  $\hat{v}_t^P$  and  $\hat{v}_t^F$  into its final prediction; we feed  $e_t^P$  and  $e_t^F$  to leverage the high-level semantics that the bidirectional video prediction network has learned. We contrast standard interpolation with TAI algebraically:

$$\hat{v}_t = \phi_{interp}(\hat{v}_t^P, \hat{v}_t^F), \quad (4)$$

$$\hat{v}_t = \phi_{TAI}(\hat{v}_t^P, e_t^P, \hat{v}_t^F, e_t^F, w_t). \quad (5)$$

Our modifications can be used to augment any existing frame interpolation network. In our case, we extend the one from Niklaus et al. [24], which generates an interpolated frame by applying a set of patch-wise kernels to the two input images, and then summing the two filtered images element-wise.

We now describe the architecture of our TAI network, shown in Fig. 2. First, we apply an encoder-decoder network to  $e_t^P$  and  $e_t^F$  to combine them into a unified embedding  $b_t$ :

$$b_t = \phi_{blend}^{enc,dec}(e_t^P, e_t^F). \quad (6)$$

Next, we augment  $b_t$  with an additional feature channel whose value at all locations equals the scaled time step  $w_t$ . We pass the result to a sequence of convolutional layers  $\phi_{blend}^{kg}$  to generate two separable 2D kernels for each pixel in the final output:

$$k_t^{P,h}, k_t^{P,v}, k_t^{F,h}, k_t^{F,v} = \phi_{blend}^{kg}([b_t, \text{tile}(w_t)]), \quad (7)$$

$$K_t^P(x, y) = k_t^{P,v}(x, y) * k_t^{P,h}(x, y), \quad (8)$$

$$K_t^F(x, y) = k_t^{F,v}(x, y) * k_t^{F,h}(x, y), \quad (9)$$

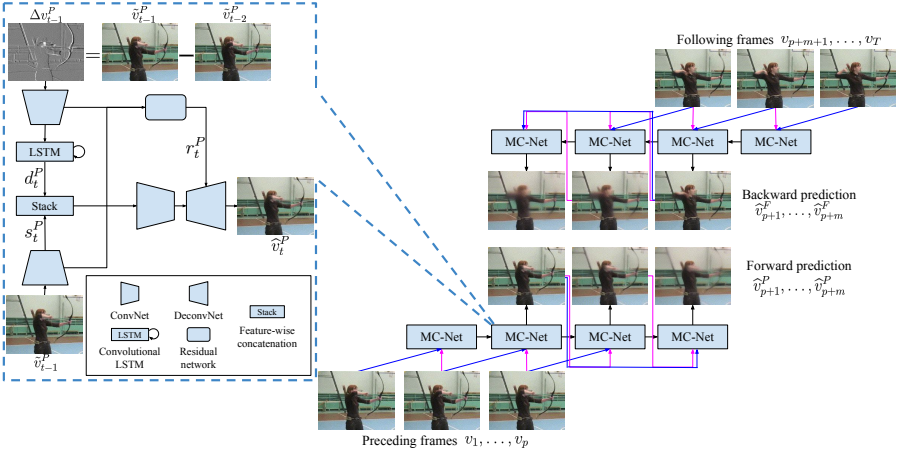


Fig. 3: The architecture of MC-Net in the context of our bidirectional video prediction process

where  $k_t^{(\cdot, \cdot)}(x, y)$  denotes the feature column of  $k_t^{(\cdot, \cdot)}$  at  $(x, y)$ , and  $K_t^{(\cdot)}(x, y)$  denotes the separable 2D kernel to apply to the patch in the forward or backward prediction that is centered at  $(x, y)$ . Finally, we apply these kernels to the patches of both intermediate predictions to obtain the final prediction  $\hat{v}_t$ :

$$\hat{v}_t(x, y) = K_t^P(x, y) * \mathcal{P}_P(x, y) + K_t^F(x, y) * \mathcal{P}_F(x, y), \quad (10)$$

where  $\hat{v}_t(x, y)$  is the value of  $\hat{v}_t$  at  $(x, y)$ , and  $\mathcal{P}_P(x, y)$  and  $\mathcal{P}_F(x, y)$  are the patches centered at  $(x, y)$  in  $\hat{v}_t^P$  and  $\hat{v}_t^F$  respectively.

### 3.2 Video Prediction Network $\phi_{pred}$

We now describe the video prediction network that we use to generate the forward and backward predictions. We implement this component with MC-Net [30], shown in Fig. 3, but note that our method is agnostic to the chosen video prediction network. For brevity, our explanation focuses on how we generate the forward prediction  $\hat{M}_V^P$ .

Let us define  $\tilde{v}_k^P$  as the available video frame from either  $P_V$  or  $\hat{M}_V^P$  at time step  $k$ , and  $\Delta v_{t-1}^P = \tilde{v}_{t-1}^P - \tilde{v}_{t-2}^P$  ( $\Delta v_{t-1}^P$  is a motion difference frame). MC-Net takes both the motion difference frame  $\Delta v_{t-1}^P$  and the full frame  $\tilde{v}_{t-1}^P$  from the previous time step as inputs, and transforms them into the next frame in the forward prediction,  $\hat{v}_t^P$ , as follows. First, it passes the full frame  $\tilde{v}_{t-1}^P$  through three convolutional layer blocks from VGGNet [31] to yield a content encoding  $s_t^P$ . Next, it encodes the motion difference frame  $\Delta v_{t-1}^P$  with three convolutional layer blocks from VGGNet (distinct from those used to obtain  $s_t^P$ ), and passes the result to a Convolutional LSTM [32], yielding a motion encoding  $d_t^P$ . Afterwards, it feeds the intermediate outputs of all VGG blocks to a CNN to yield a set of “motion-content residuals”  $r_t^P$ . Finally, it stacks  $s_t^P$  and  $d_t^P$  together and feeds

the result, along with  $r_t^P$ , to an encoder-decoder network to produce the next forward prediction  $\widehat{v}_t^P$ .

For all middle time steps  $t \in \{p+1, \dots, p+m\}$ , we store the forward prediction frames  $\widehat{v}_t^P$ , content encodings  $s_t^P$ , motion encodings  $d_t^P$ , and motion-content residuals  $r_t^P$ . We repeat the same process on  $F_V^R$  and  $(\widehat{M}_V^F)^R$ , using the same weights for MC-Net, to obtain the corresponding information for the backward prediction  $\widehat{v}_t^F$ ,  $s_t^F$ ,  $d_t^F$ , and  $r_t^F$  for the same middle time steps. The intermediate activations that we feed to the TAI network are  $e_t^P = \{s_t^P, d_t^P, r_t^P\}$  and  $e_t^F = \{s_t^F, d_t^F, r_t^F\}$ . We encourage the reader to read Villegas et al. [30] for more details on their network architecture.

### 3.3 Training Strategy

To train our complete video frame inpainting model, we use adversarial training, which has been shown in Mathieu et al. [33] to improve the sharpness of predictions. In our case, we train a discriminator  $D$ , a binary classification CNN, to distinguish between clips from the dataset and clips generated by our model. Meanwhile, we train our model—the “generator”—to not only fool the discriminator, but also to generate predictions that resemble the ground truth.

We update the generator and the discriminator in an alternating fashion. In the generator update step, we update our model by minimizing the following structured loss:

$$\begin{aligned} \mathcal{L}_g = \alpha & \left[ \mathcal{L}_{img}(\widehat{M}_V^P, M_V) + \mathcal{L}_{img}(\widehat{M}_V^F, M_V) + \mathcal{L}_{img}(\widehat{M}_V, M_V) \right] \\ & + \beta \mathcal{L}_{GAN}(\widehat{M}_V), \end{aligned} \quad (11)$$

$$\mathcal{L}_{GAN}(\widehat{M}_V) = -\log D([P_V, \widehat{M}_V, F_V]), \quad (12)$$

where  $\alpha$  and  $\beta$  are hyperparameters to balance the contribution of the reconstruction-based loss  $\mathcal{L}_{img}$  and the adversarial loss  $\mathcal{L}_{GAN}$ . Note that we supervise both the final prediction  $\widehat{M}_V$  and the intermediate predictions  $\widehat{M}_V^P$  and  $\widehat{M}_V^F$  simultaneously. The loss  $\mathcal{L}_{img}$  consists of the squared-error loss  $\mathcal{L}_2$  and the image gradient difference loss  $\mathcal{L}_{gdl}$  defined in Mathieu et al. [33]:

$$\mathcal{L}_{img}(\widehat{M}_V^{(\cdot)}, M_V) = \mathcal{L}_2(\widehat{M}_V^{(\cdot)}, M_V) + \mathcal{L}_{gdl}(\widehat{M}_V^{(\cdot)}, M_V), \quad (13)$$

$$\mathcal{L}_2(\widehat{M}_V^{(\cdot)}, M_V) = \sum_{t=p+1}^{p+m} \left\| v_t - \widehat{v}_t^{(\cdot)} \right\|_2^2, \quad (14)$$

$$\begin{aligned} \mathcal{L}_{gdl}(\widehat{M}_V^{(\cdot)}, M_V) = \sum_{t=p+1}^{p+m} \sum_{i,j}^{h,w} & \left( \left| |v_t(i,j) - v_t(i-1,j)| - |\widehat{v}_t^{(\cdot)}(i,j) - \widehat{v}_t^{(\cdot)}(i-1,j)| \right| \right. \\ & \left. + \left| |v_t(i,j-1) - v_t(i,j)| - |\widehat{v}_t^{(\cdot)}(i,j-1) - \widehat{v}_t^{(\cdot)}(i,j)| \right| \right). \end{aligned} \quad (15)$$

Here,  $\widehat{M}_V^{(\cdot)}$  can be one of the intermediate predictions  $\{\widehat{M}_V^P, \widehat{M}_V^F\}$  or the final prediction  $\widehat{M}_V$ . In the discriminator update step, we update the discriminator by minimizing the cross-entropy error:

$$\mathcal{L}_d = -\log D\left([P_V, M_V, F_V]\right) - \log\left(1 - D\left([P_V, \widehat{M}_V, F_V]\right)\right). \quad (16)$$

We use the same discriminator as Villegas et al. [30], but replace each layer that is followed by batch normalization [34] with a spectral normalization layer [35], which we have found results in more accurate predictions.

## 4 Experiments

### 4.1 Baselines

We introduce two classes of baselines for the video frame inpainting problem. In the first class, instead of learning a function  $\phi$ , we hand-craft several  $\phi$ 's that can perform well on certain video prediction tasks, particularly on videos with little movement or periodic motion. The baselines described by Eqs. 17-19 copy or take a simple average of the last preceding frame  $v_p$  and the first following frame  $v_{p+m+1}$ :

$$\phi_{\text{repeat\_P}}(P_V, F_V) = \{v_p, v_p, \dots, v_p\}, \quad (17)$$

$$\phi_{\text{repeat\_F}}(P_V, F_V) = \{v_{p+m+1}, v_{p+m+1}, \dots, v_{p+m+1}\}, \quad (18)$$

$$\phi_{\text{SA\_P\_F}}(P_V, F_V) = \{\widehat{v}, \widehat{v}, \dots, \widehat{v}\}, \text{ where } \widehat{v} = \frac{v_p + v_{p+m+1}}{2}. \quad (19)$$

Also, we try incorporating the scaled time step of the predicted frame  $w_t = (t - p)/(m + 1)$  by computing a time-weighted average of  $v_p$  and  $v_{p+m+1}$ :

$$\phi_{\text{TW\_P\_F}}(P_V, F_V) = \{\widehat{v}_{p+1}, \widehat{v}_{p+2}, \dots, \widehat{v}_{p+m}\}, \quad (20)$$

$$\widehat{v}_t = (1 - w_t)v_p + w_tv_{p+m+1}. \quad (21)$$

In the second class of baselines, we highlight the value of our TAI module by proposing two bidirectional prediction models that blend each frame from the forward prediction  $\widehat{M}_V^P$  and the backward prediction  $\widehat{M}_V^F$  without an interpolation network. Instead, they blend by computing either a simple average (bi-SA, Eq. 22) or a weighted average based on the scaled time step  $w_t$  (bi-TW, Eq. 23):

$$\widehat{v}_t = \frac{\widehat{v}_t^P + \widehat{v}_t^F}{2}, \quad (22)$$

$$\widehat{v}_t = (1 - w_t)\widehat{v}_t^P + w_t\widehat{v}_t^F. \quad (23)$$

### 4.2 Datasets

We evaluate each video frame inpainting model on videos from three human action datasets: KTH Actions [36], HMDB-51 [37], and UCF-101 [38]. KTH



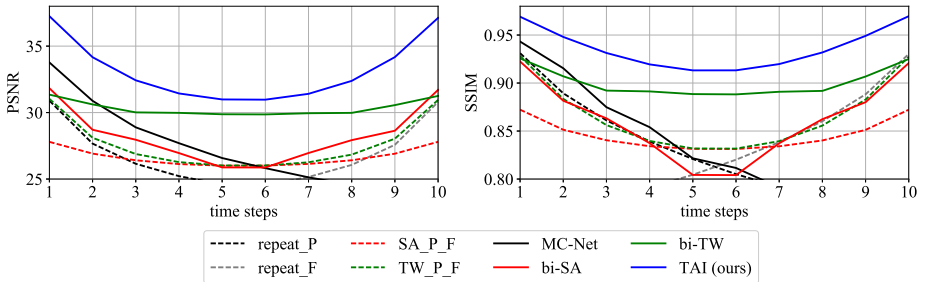


Fig. 4: Quantitative results on the KTH Actions dataset (for both PSNR and SSIM, higher is better). We compare our full model (TAI) to the baselines described in Sec. 4.1

Actions contains a total of 2,391 grayscale videos with resolution 120 x 160 (height x width) across six action classes; it also provides a standard training and testing set. We divide the standard training set into a smaller training set and a validation set; the former is used to train our models, and the latter is used for hyperparameter search. Due to memory constraints, we reduce the resolution to 128 x 128. We train each model to predict five middle frames from five preceding and five following frames; at inference time, each model is evaluated on its ability to predict ten middle frames from five preceding and five following frames.

HMDB-51 contains 6,849 RGB videos across 51 action classes; each video has a fixed height of 240 pixels. The dataset provides three cross-validation folds (each including a training and a test set); we take the test videos from the first fold as our test set and separate the remaining videos into our training and validation sets. Due to memory constraints, we reduce the resolution of each video to 160 x 208, and train each model to predict three middle frames from four preceding and four following frames. At test time, we take in the same number of preceding/following frames, but predict five frames in the middle.

UCF-101 contains 13,320 RGB videos with resolution 240 x 320 across 101 action classes. It provides three cross-validation folds for action recognition; we take the test videos from the first fold as our test set and divide the remaining videos into our training and validation sets. The remainder of our experimental setup for UCF-101 matches our setup for HMDB-51.

### 4.3 KTH Actions

To evaluate the performance of the proposed baselines and our full model with the TAI network (we refer to this full model as TAI for brevity), we follow existing video prediction literature [30,33] by reporting the Structural Similarity (SSIM) [39] and Peak Signal-to-Noise Ratio (PSNR) between each predicted frame and the ground truth. We draw a series of conclusions from the quantitative comparison shown in Fig. 4. First, the low performance of the hand-crafted baselines (the dashed curves in Fig. 4) indicate that our task is challenging, and

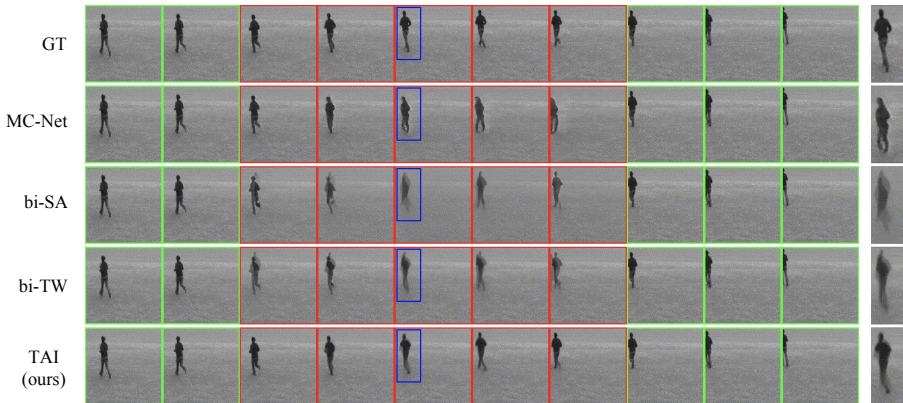


Fig. 5: Comparison of predictions from our TAI model to baseline methods (Sec. 4.1) on KTH Actions. We visualize every other frame of the input and predicted sequences. Refer to the supplementary materials for more results

requires a model that generates a *non-trivial* prediction from *multiple* preceding and following frames. Second, the performance of MC-Net drops quickly over time due to its lack of guidance from the following frames. Third, between the bidirectional prediction baselines, bi-TW does a better job than bi-SA since it incorporates the scaled time step  $w_t$  via a hand-crafted, time-weighted average. Finally, TAI outperforms bi-TW because it learns a complex blending function that leverages both time step information and intermediate activations from the bidirectional video prediction module.

In Fig. 5, we visualize the predictions made by MC-Net, bi-SA, bi-TW, and TAI (we encourage the reader to view additional results in the supplementary materials). MC-Net generates blob-like poses that fail to preserve the proper shape of the body and are inconsistent with the following frames. Meanwhile, bi-SA and bi-TW generate frames with a noticeable “ghosting” effect (e.g. both predictions contain two torsos overlapping with each other), leading to a drop in PSNR and SSIM scores. On the other hand, TAI overcomes these challenges: its predictions are consistent with both the preceding and following frames, and they contain one unified, well-shaped torso. We have found that SSIM drops more drastically than PSNR when ghosting occurs, indicating that it is a better evaluation metric for our purposes.

#### 4.4 Qualitative Analysis of Blending Methods

Next, we compare the forward and backward predictions to the final prediction for bi-SA, bi-TW, and TAI in order to highlight the benefit of a learned blending function over a hand-crafted one. Across all three models, the forward prediction is inconsistent with the backward one for most videos. For instance, in Fig. 6, the scale of the actor always differs between the forward and backward predictions. However, the quality of the final prediction improves with the complexity of the blending strategy. For example, since bi-SA blends the two predictions evenly, we

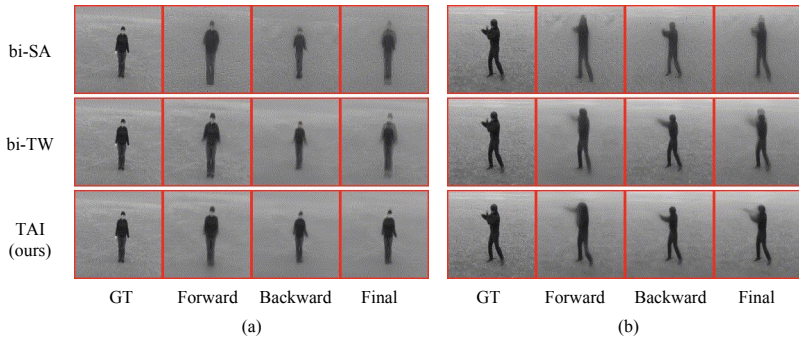


Fig. 6: Comparison of the forward, backward, and final predictions for the third middle frame (of ten) of two videos

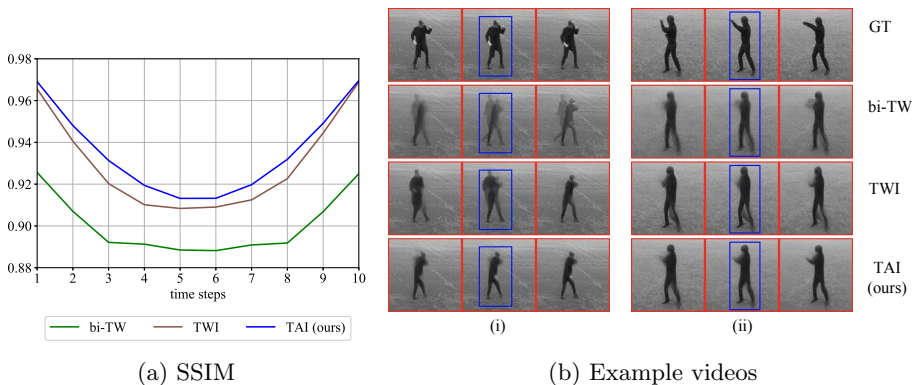


Fig. 7: Ablative comparison between bi-TW, TWI, and our full TAI model. Higher SSIM is better

observe in the final prediction for Fig. 6a a blurry background and two outlines of the actor’s body; in Fig. 6b, we see the outlines of two heads. bi-TW produces similar artifacts to bi-SA for both videos, but its final predictions are clearer. Finally, TAI reconciles the differences between the forward and backward predictions without introducing ghosting artifacts: in Fig. 6a, the final prediction compromises between the actor’s sizes from the intermediate predictions, and in Fig. 6b, the difference in the actor’s head position is resolved, resulting in a clean outline of the head. We conclude that even though all three methods generate inconsistent forward and backward predictions, TAI can successfully reconcile the differences to generate a crisp final prediction.

#### 4.5 Ablation Studies

Feeding time information into the blending network such that it can *learn* to use that information most effectively is key to generating high-quality predictions. To verify this, we replace the blending module with a time-agnostic interpolation network and apply a time-weighted average to its outputs; we call this version the

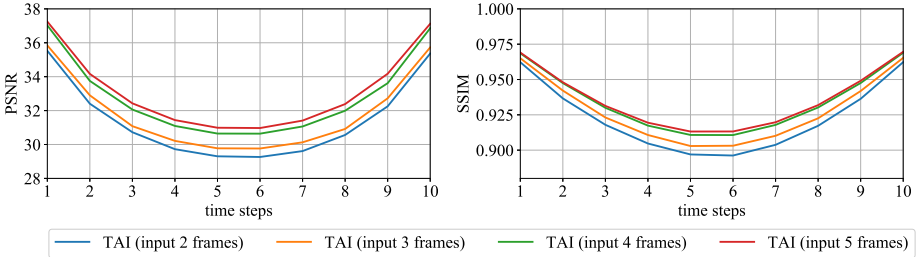


Fig. 8: Performance of our trained model with two, three, four, and five preceding and following frames at test time on the KTH Actions dataset. Higher PSNR and SSIM is better

time-weighted interpolation (TWI) network. In Fig. 7, we compare bi-TW, TAI, and a bidirectional video prediction model with TWI. We see that TWI performs better than bi-TW both quantitatively and qualitatively because the ghosting artifacts in its predictions are less apparent. However, it still incorporates time information with a hand-crafted function, which prevents TWI from completely avoiding ghosting artifacts. For example, TWI generates two torsos in Fig. 7b (i) and a fake leg between two legs in Fig. 7b (ii). On the other hand, TAI avoids ghosting artifacts more successfully than TWI: for both videos in Fig. 7b, we see that TAI generates a clear, sharp outline around the actor without introducing artificial torsos or limbs.

## 4.6 Importance of Context Frames

In this section, we show our model’s ability to leverage the context information from the preceding and the following sequences which, as argued in Sec. 1, is vital to performing well on the video frame inpainting task. In Fig. 8, we plot the quantitative performance of our trained model as we increase the number of available frames at test time from two to five (recall that we train our model on five preceding and following frames). Our model obtains progressively better PSNR and SSIM values as we increase the number of preceding and following frames; this shows that our model successfully leverages the increasing amount of context information to improve its predictions.

## 4.7 HMDB-51 and UCF-101

We conclude our experiments by demonstrating our model’s ability to perform well on complex videos depicting challenging scenes and a wide variety of actions. We do this by comparing our full TAI model to the baselines proposed in Sec. 4.1 on videos from HMDB-51 and UCF-101. We see from the quantitative results in Fig. 9 that none of the baselines outperform the others by a definitive margin. This contrasts with our findings in Sec. 4.3 where we found that for KTH Actions, bi-TW produces substantially better predictions than all the other baselines.

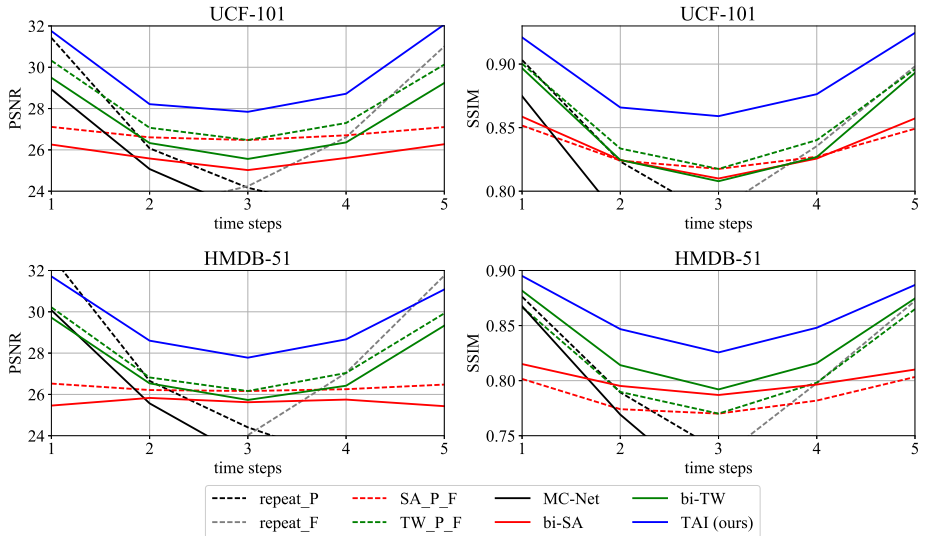


Fig. 9: Quantitative results on the UCF-101 and HMDB-51 datasets (higher PSNR and SSIM is better). We compare our method to the baselines described in Sec. 4.1

We note that the biggest difference between KTH Actions and HMDB-51/UCF-101 is that the scenes in HMDB-51 and UCF-101 are far more complex than in KTH Actions; this suggests that bi-TW performs poorly when observing complex scenes. However, our model still outperforms all baselines on HMDB-51 and UCF-101, suggesting that it is best equipped for handling complex videos.

We present qualitative comparisons in Fig. 10. In Fig. 10a, we observe two contours of the girl’s hair in the bi-SA prediction, and a blurry facial expression in the bi-TW prediction. On the other hand, our TAI model generates a unified contour of the hair and a clear facial expression at the same time step. Moving on to Fig. 10b, we note that MC-Net distorts the background in the later middle frames, and that both bi-SA and bi-TW generate blurry patterns on the man’s jacket and pants. However, TAI produces a clear white stripe on the man’s pants, as well as a sharp outline around his jacket. More qualitative comparisons for UCF-101 and HMDB-51 are included in the supplementary materials. Our results demonstrate that on video datasets containing complex scenes and a large number of action classes, TAI generates predictions that are more visually satisfying than several strong baselines.

## 5 Conclusion

In this paper, we have tackled the video frame inpainting problem by generating two sets of intermediate predictions conditioned on the preceding and following frames respectively, and then blending them together with our novel TAI network. Our experiments on KTH Actions, HMDB-51, and UCF-101 show that our





Fig. 10: Comparison of predictions from our approach to baseline methods (Sec. 4.1) on the UCF-101 and HMDB-51 datasets. We visualize every second frame of the input and predicted sequences. Refer to the supplementary materials for more results

method generates more accurate and visually pleasing predictions than multiple strong baselines. Furthermore, our in-depth analysis has revealed that our TAI network successfully leverages time step information to reconcile inconsistencies in the intermediate predictions, and that it leverages the full context provided by the preceding and following frames.

In future work, we aim to improve performance by exploiting semantic knowledge about the video content, e.g. by modeling human poses or the periodicity of certain actions. We also aim to explore models that can predict an even greater number of frames, i.e. several seconds of video instead of fractions of a second. We hope that our work inspires innovations in deep learning for not only video frame inpainting, but also general video inpainting, frame interpolation, and video prediction.

## References

1. Bertalmio, M., Bertozzi, A.L., Sapiro, G.: Navier-Stokes, Fluid Dynamics, And Image And Video Inpainting. In: IEEE Conference on Computer Vision and Pattern Recognition. (2001)
2. Hays, J., Efros, A.A.: Scene Completion Using Millions Of Photographs. In: ACM Transactions on Graphics. Volume 26. (2007) 4
3. Komodakis, N., Tziritis, G.: Image Completion Using Global Optimization. In: IEEE Conference on Computer Vision and Pattern Recognition. (2006)
4. He, K., Sun, J.: Statistics Of Patch Offsets For Image Completion. In: European Conference on Computer Vision. (2012) 16–29
5. Lahiri, A., Jain, A., Biswas, P.K., Mitra, P.: Improving Consistency and Correctness of Sequence Inpainting using Semantically Guided Generative Adversarial Network. arXiv preprint arXiv:1711.06106 (2017)
6. Pathak, D., Krahenbuhl, P., Donahue, J., Darrell, T., Efros, A.A.: Context Encoders: Feature Learning By Inpainting. In: IEEE Conference on Computer Vision and Pattern Recognition. (2016) 2536–2544
7. Yeh, R.A., Chen, C., Lim, T.Y., Schwing, A.G., Hasegawa-Johnson, M., Do, M.N.: Semantic Image Inpainting With Deep Generative Models. In: IEEE Conference on Computer Vision and Pattern Recognition. (2017) 5485–5493
8. Yang, C., Lu, X., Lin, Z., Shechtman, E., Wang, O., Li, H.: High-Resolution Image Inpainting Using Multi-scale Neural Patch Synthesis. In: IEEE Conference on Computer Vision and Pattern Recognition. (2017)
9. Demir, U., Unal, G.: Deep Stacked Networks with Residual Polishing for Image Inpainting. arXiv preprint arXiv:1801.00289 (2017)
10. Wexler, Y., Shechtman, E., Irani, M.: Space-Time Video Completion. In: IEEE Conference on Computer Vision and Pattern Recognition. (2004)
11. Jia, Y.T., Hu, S.M., Martin, R.R.: Video Completion Using Tracking And Fragment Merging. *The Visual Computer* **21**(8-10) (2005) 601–610
12. Shen, Y., Lu, F., Cao, X., Foroosh, H.: Video Completion For Perspective Camera Under Constrained Motion. In: International Conference on Pattern Recognition. Volume 3. (2006) 63–66
13. Newson, A., Almansa, A., Fradet, M., Gousseau, Y., Pérez, P.: Video Inpainting Of Complex Scenes. *SIAM Journal on Imaging Sciences* **7**(4) (2014) 1993–2019
14. Patwardhan, K.A., Sapiro, G., Bertalmío, M.: Video Inpainting Under Constrained Camera Motion. *IEEE Transactions on Image Processing* **16**(2) (2007) 545–553
15. Jia, J., Tai-Pang, W., Tai, Y.W., Tang, C.K.: Video Repairing: Inference Of Foreground And Background Under Severe Occlusion. In: IEEE Conference on Computer Vision and Pattern Recognition. (2004)
16. Cheung, V., Frey, B.J., Jovic, N.: Video Epitomes. *International Journal of Computer Vision* **76**(2) (2008) 141–152
17. Granados, M., Kim, K.I., Tompkin, J., Kautz, J., Theobalt, C.: Background Inpainting For Videos With Dynamic Objects And A Free-Moving Camera. In: European Conference on Computer Vision. (2012) 682–695
18. Ebdelli, M., Le Meur, O., Guillemot, C.: Video Inpainting With Short-term Windows: Application To Object Removal And Error Concealment. *IEEE Transactions on Image Processing* **24**(10) (2015) 3034–3047
19. Borzi, A., Ito, K., Kunisch, K.: Optimal Control Formulation For Determining Optical Flow. *SIAM Journal On Scientific Computing* **24**(3) (2003) 818–847

20. Chen, K., Lorenz, D.A.: Image Sequence Interpolation Using Optimal Control. *Journal of Mathematical Imaging and Vision* **41**(3) (2011) 222–238
21. Werlberger, M., Pock, T., Unger, M., Bischof, H.: Optical flow guided TV-L1 video interpolation and restoration. In: *International Workshop on Energy Minimization Methods in Computer Vision and Pattern Recognition*. (2011) 273–286
22. Long, G., Kneip, L., Alvarez, J.M., Li, H., Zhang, X., Yu, Q.: Learning Image Matching By Simply Watching Video. In: *European Conference on Computer Vision*. (2016) 434–450
23. Niklaus, S., Mai, L., Liu, F.: Video Frame Interpolation Via Adaptive Convolution. In: *IEEE International Conference on Computer Vision*. Volume 2. (2017) 6
24. Niklaus, S., Mai, L., Liu, F.: Video Frame Interpolation via Adaptive Separable Convolution. In: *IEEE Conference on Computer Vision and Pattern Recognition*. (2017) 261–270
25. Liu, Z., Yeh, R., Tang, X., Liu, Y., Agarwala, A.: Video Frame Synthesis Using Deep Voxel Flow. In: *International Conference on Computer Vision (ICCV)*. Volume 2. (2017)
26. Ranzato, M., Szlam, A., Bruna, J., Mathieu, M., Collobert, R., Chopra, S.: Video (Language) Modeling: A Baseline For Generative Models Of Natural Videos. arXiv preprint arXiv:1412.6604 (2014)
27. Srivastava, N., Mansimov, E., Salakhudinov, R.: Unsupervised Learning Of Video Representations Using LSTMs. In: *International Conference On Machine Learning*. (2015) 843–852
28. Lotter, W., Kreiman, G., Cox, D.: Deep Predictive Coding Networks for Video Prediction and Unsupervised Learning. In: *International Conference on Learning Representations*. (2017)
29. Kalchbrenner, N., Oord, A.v.d., Simonyan, K., Danihelka, I., Vinyals, O., Graves, A., Kavukcuoglu, K.: Video Pixel Networks. In: *International Conference On Machine Learning*. (2017)
30. Villegas, R., Yang, J., Hong, S., Lin, X., Lee, H.: Decomposing Motion And Content For Natural Video Sequence Prediction. In: *International Conference on Learning Representations*. (2017)
31. Simonyan, K., Zisserman, A.: Very Deep Convolutional Networks for Large-Scale Image Recognition. In: *International Conference on Learning Representations*. (2015)
32. Shi, X., Chen, Z., Wang, H., Yeung, D.Y., Wong, W.K., Woo, W.C.: Convolutional Lstm Network: A Machine Learning Approach For Precipitation Nowcasting. In: *Advances In Neural Information Processing Systems*. (2015) 802–810
33. Mathieu, M., Couprie, C., LeCun, Y.: Deep Multi-Scale Video Prediction Beyond Mean Square Error. In: *International Conference on Learning Representations*. (2016)
34. Ioffe, S., Szegedy, C.: Batch Normalization: Accelerating Deep Network Training by Reducing Internal Covariate Shift. In: *International Conference On Machine Learning*. (2015) 448–456
35. Miyato, T., Kataoka, T., Koyama, M., Yoshida, Y.: Spectral Normalization for Generative Adversarial Networks. In: *International Conference on Learning Representations*. (2018)
36. Schuldt, C., Laptev, I., Caputo, B.: Recognizing Human Actions: A Local Svm Approach. In: *International Conference on Pattern Recognition*. Volume 3. (2004) 32–36



37. Kuehne, H., Jhuang, H., Garrote, E., Poggio, T., Serre, T.: HMDB: A Large Video Database For Human Motion Recognition. In: IEEE International Conference on Computer Vision. (2011) 2556–2563
38. Soomro, K., Zamir, A.R., Shah, M.: UCF101: A Dataset Of 101 Human Actions Classes From Videos In The Wild. CRCV-TR-12-01 (2012)
39. Wang, Z., Bovik, A.C., Sheikh, H.R., Simoncelli, E.P.: Image Quality Assessment: From Error Visibility To Structural Similarity. IEEE Transactions on Image Processing **13**(4) (2004) 600–612
40. Kingma, D.P., Ba, J.L.: ADAM: A Method For Stochastic Optimization. In: International Conference on Learning Representations. (2015)
41. Glorot, X., Bengio, Y.: Understanding the difficulty of training deep feedforward neural networks. In: Proceedings of the Thirteenth International Conference on Artificial Intelligence and Statistics. (2010) 249–256

# A Temporally-Aware Interpolation Network for Video Frame Inpainting: Supplementary materials

## A Qualitative Results on KTH Actions

In this section, we give six more qualitative results on the KTH Actions dataset, one for each action class. To save space, we visualize every other frame. Our full model TAI gives more visually pleasing predictions on all six classes than MC-Net, bi-SA and bi-TW.



Fig. 11: Comparison on a “boxing” video from KTH Actions



Fig. 12: Comparison on a “handclapping” video from KTH Actions

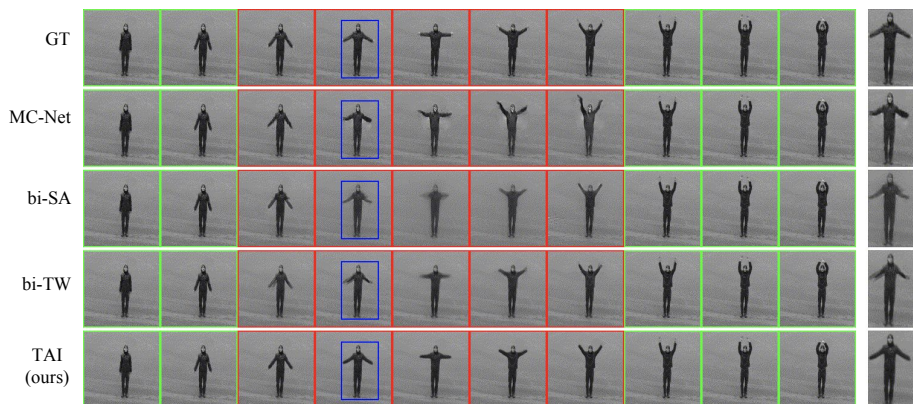


Fig. 13: Comparison on a “handwaving” video from KTH Actions

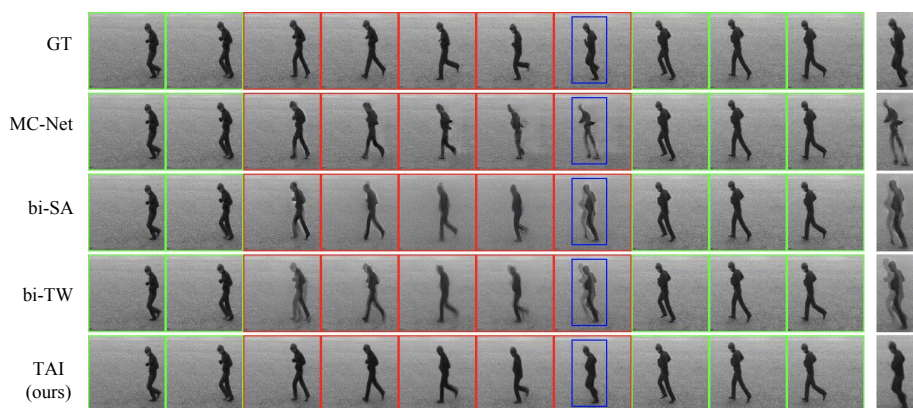


Fig. 14: Comparison on a “jogging” video from KTH Actions

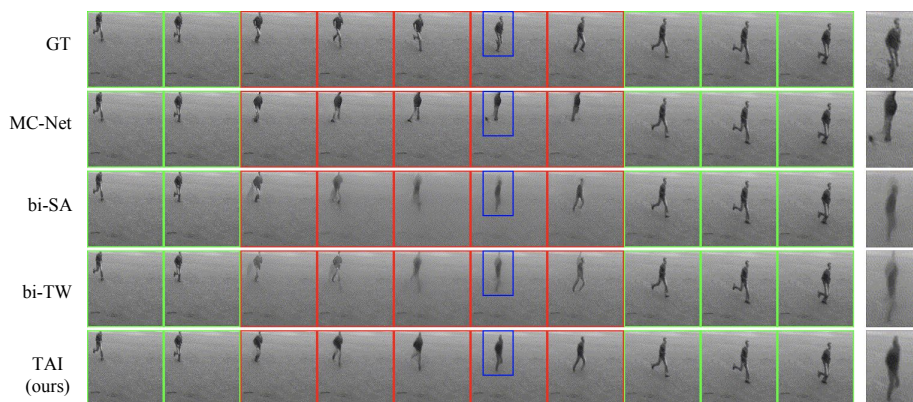


Fig. 15: Comparison on a “running” video from KTH Actions





Fig. 16: Comparison on a “walking” video from KTH Actions

## B Qualitative Results on UCF-101 and HMDB-51

In this section, we give six more qualitative results on different action classes, three from UCF-101 and three from HMDB-51. To save space, we visualize every other frame. Our full model TAI reconciles the misalignment of the forward and backward predictions and gives a crisp prediction.



Fig. 17: Comparison on a “Skijet” video from UCF-101



Fig. 18: Comparison on a “RopeClimbing” video from UCF-101

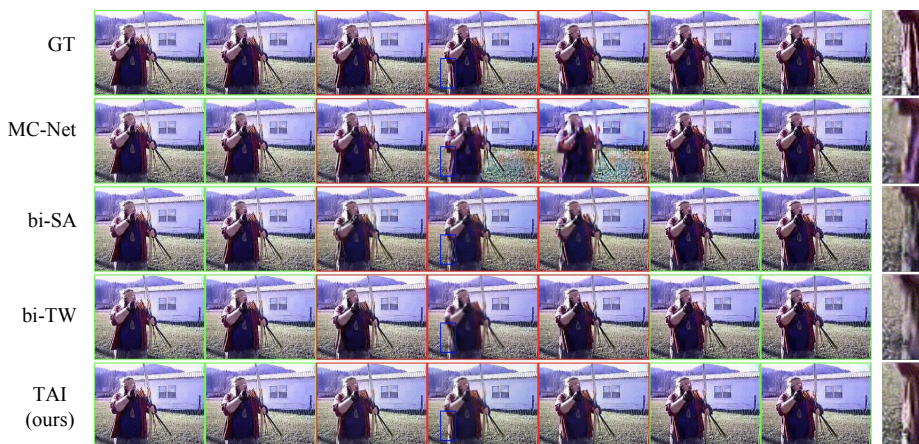


Fig. 19: Comparison on an “Archery” video from UCF-101

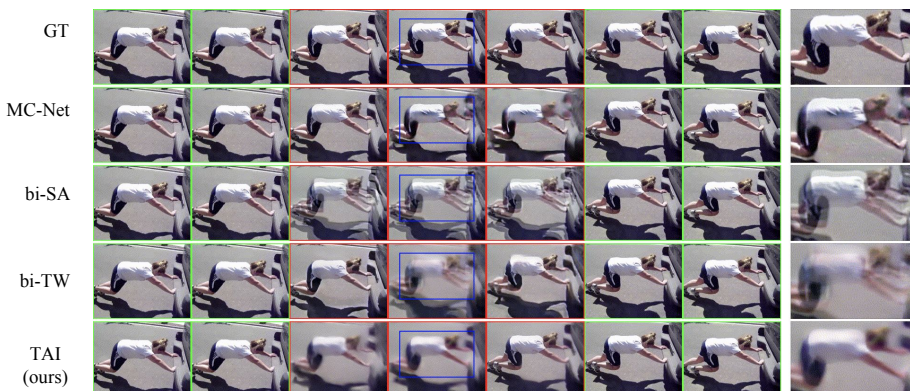


Fig. 20: Comparison on a “push” video from HMDB-51





Fig. 21: Comparison on a “jump” video from HMDB-51

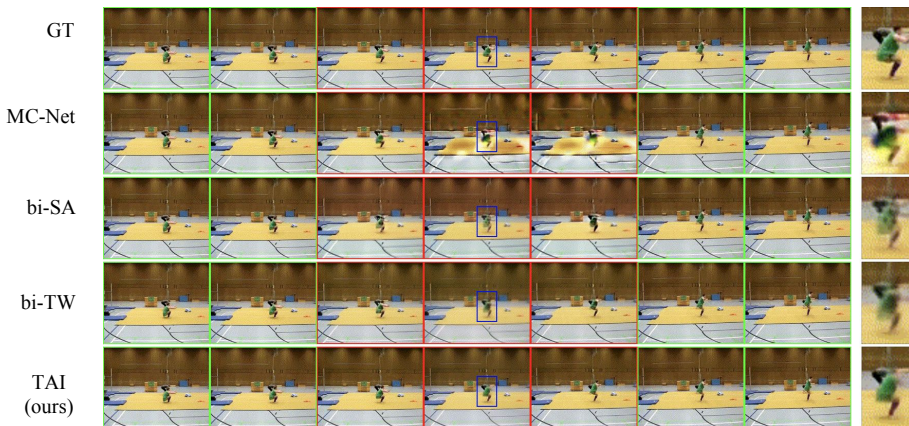


Fig. 22: Comparison on a “somersault” video from HMDB-51

## C Importance of Context Frames: Qualitative Analysis

In addition to the quantitative results in the main paper, we provide the qualitative results on the KTH Actions dataset to demonstrate that our TAI model can leverage the context information from the preceding and following frames to better predict the middle frames.

Comparisons in Fig. 23 show how the final prediction changes when our model takes in a varying number of preceding and following frames at test time. When our model takes in only two frames from the preceding and following sequences, the prediction of the middle sequence fails to give one unified location for the actor due to the limited amount of available context information; however, when it takes in five frames, the final prediction contains much fewer ghosting artifacts. These results demonstrate that our TAI model can leverage the context

information from multiple preceding and following frames to enhance the quality of the final prediction.

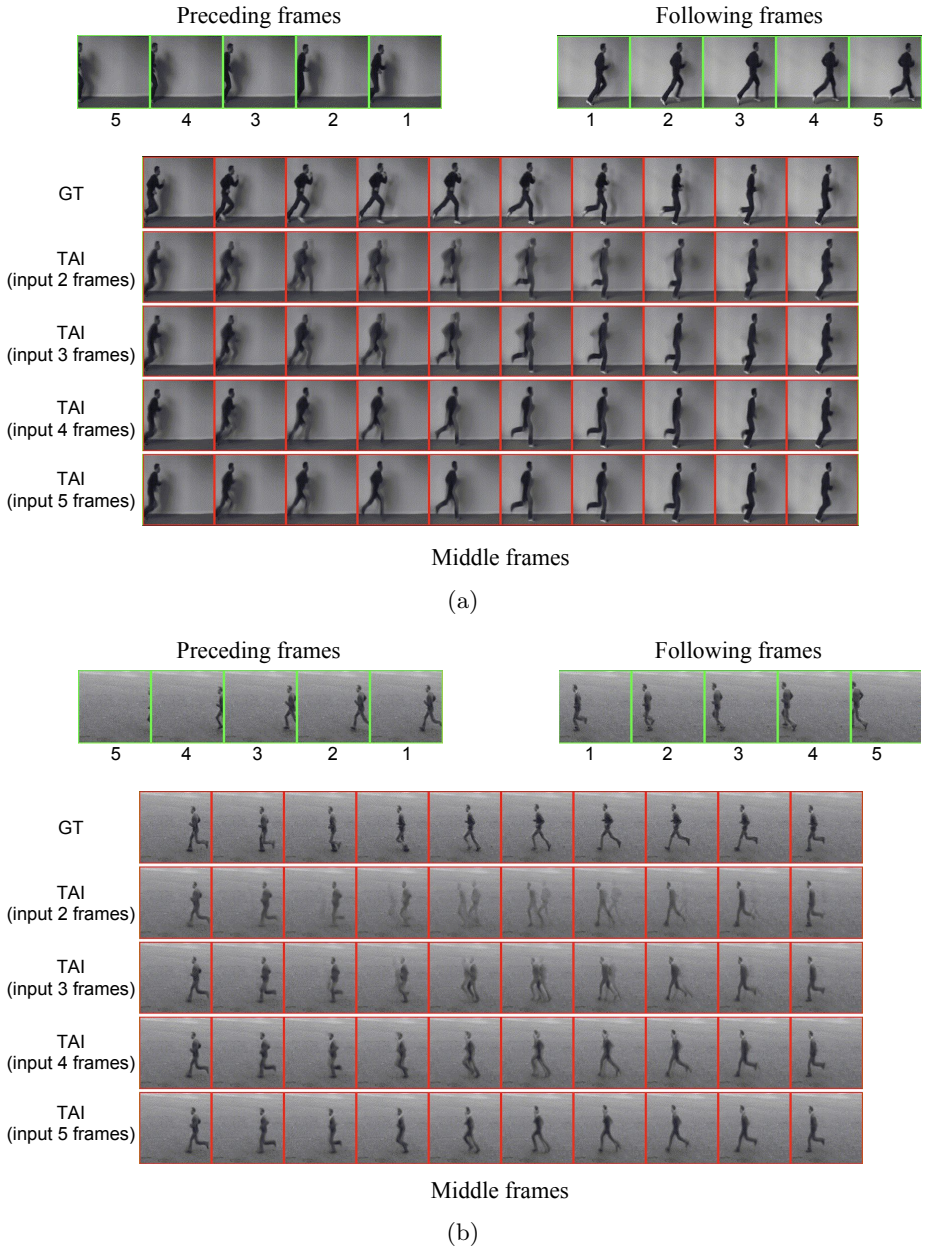


Fig. 23: Qualitative results of our trained TAI model taking in two, three, four and five preceding and following frames at test time on the KTH Actions Dataset

## D Comparison of Trained Models for Variable Number of Middle Frames

In this section, we demonstrate that our TAI model generates higher-quality predictions of the middle frames than MC-Net, bi-SA, and bi-TW across a variable number of middle frames to inpaint. To do this, we take all four models, which were all trained to predict five middle frames, and compare their performance when predicting six, seven, eight, or nine middle frames at test time on the KTH Actions dataset. From Fig. 24, we observe that our model yields higher PSNR and SSIM values than the other models when we increase the number of outputs from six to nine at the test time. This suggests that TAI incorporates the scaled time location in a way that generalizes to a variable number of middle frames, even though it has only seen scaled time locations corresponding to five middle frames.

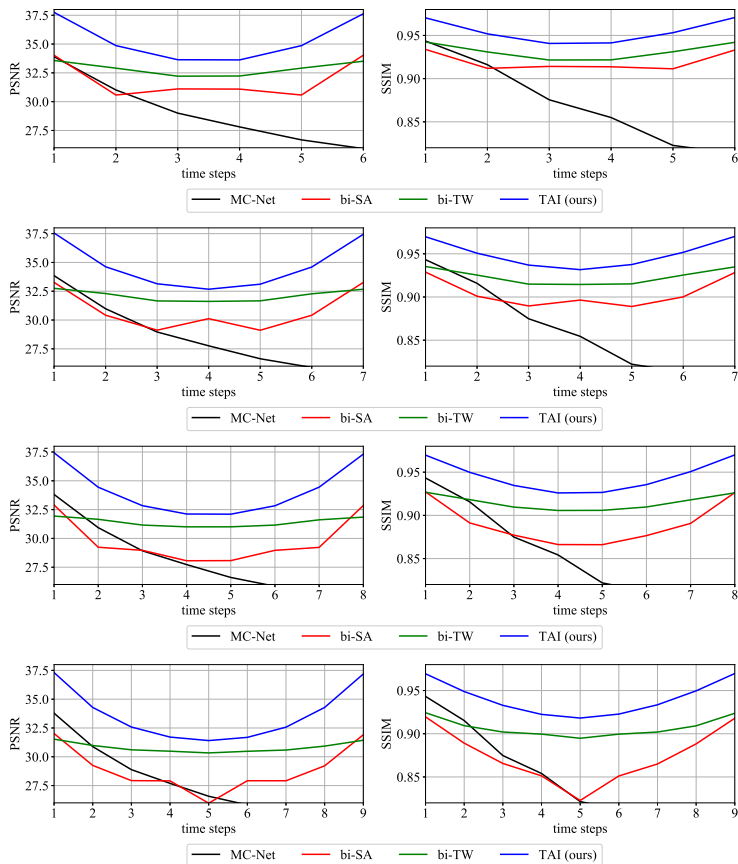


Fig. 24: Comparison of our trained model TAI with baselines when predicting 6-9 middle frames at test time on the KTH Actions dataset. Higher PSNR and SSIM is better



## E Architecture, Training, and Evaluation Details

### E.1 Model Architecture

For the video prediction module, we use the same architecture as Villegas et al. [30]. As for our TAI module, the encoder is a chain of two VGG blocks [31] and the decoder is a chain of four VGG blocks. The kernel generation part,  $\phi_{blend}^{kg}$ , contains four independent sub-networks that each predict one 1D kernel. The details of each VGG block are described in Table 1. The inputs of decoder 2 and decoder 1 are the element-wise sum of: (i) the output of the previous decoder layer, and (ii) the residual activation from the video prediction module with matching resolution.

Table 1: Architecture of TAI network

block name	type	kernel size	input channels	output channels	activation
encoder 1	conv	3x3	1024	256	RELU
	conv	3x3	256	256	RELU
	conv	3x3	256	256	RELU
	max pooling				
encoder 2	conv	3x3	256	512	RELU
	conv	3x3	512	512	RELU
	conv	3x3	512	512	RELU
	max pooling				
decoder 4	conv	3x3	512	512	RELU
	conv	3x3	512	512	RELU
	conv	3x3	512	512	RELU
	bilinear unsampling				
decoder 3	conv	3x3	512	256	RELU
	conv	3x3	256	256	RELU
	conv	3x3	256	256	RELU
	bilinear unsampling				
decoder 2	conv	3x3	256	128	RELU
	conv	3x3	128	128	RELU
	conv	3x3	128	128	RELU
	bilinear unsampling				
decoder 1	conv	3x3	128	64	RELU
	conv	3x3	64	64	RELU
	conv	3x3	64	64	RELU
	bilinear unsampling				
kernel generation x4	conv	3x3	65	64	RELU
	conv	3x3	64	64	RELU
	conv	3x3	64	51	RELU
	bilinear unsampling				

### E.2 Training, Validation, and Test Set Construction

During training, we construct minibatches by first selecting clips with  $T$  frames randomly from the videos in the training set, where  $T = p + m + f$ , and then

splitting each clip into  $p$  preceding,  $m$  middle, and  $f$  following frames. For KTH Actions,  $p = m = f = 5$ ; for HMDB-51 and UCF-101,  $p = f = 4$  and  $m = 3$ . To augment the training data, each video clip is randomly flipped horizontally or time-reversed. To validate a model, we take the first  $T$  frames from each video in the validation set and split the clips into  $p$  preceding,  $m$  middle, and  $f$  following frames.

We construct the test set differently for each dataset. For KTH Actions, we extract all clips from a sliding window of size  $T' = p + m' + f$  and stride  $s$  across all test videos, and then split each clip into  $p$  preceding,  $m'$  middle, and  $f$  following frames. In our experiments,  $p = f = 5$ ,  $m' = 10$ , and  $s$  depends on the action class ( $s = 3$  for the running and jogging classes, and  $s = m'$  for the walking, boxing, handclapping, and handwaving classes, following the stride selection process used by Villegas et al. [30]). For HMDB-51 and UCF-101, we only evaluate each model on the first  $T'$  frames of each video in the test set, where  $T' = p + m' + f$ ,  $p = f = 4$ , and  $m' = 5$ . We do not evaluate on all possible clips due to the large number of test videos in these datasets.

### E.3 Training Hyperparameters

We train the bi-SA, bi-TW, TWI and TAI models for 100,000 iterations with batch size 4. We train MC-Net for 200,000 iterations with the same batch size because it effectively receives less data per minibatch than the other models (it does not explicitly receive the following frames, unlike the other models). We use the Adam optimizer [40] with initial learning rate  $\alpha = 10^{-4}$ , first decay rate  $\beta_1 = 0.5$ , and second decay rate  $\beta_2 = 0.999$ . In the generator loss, we set the weight of the reconstruction losses  $\alpha$  to 1, and the weight of the adversarial loss  $\beta$  to 0.002. We assume our discriminator can be represented as a 3-Lipschitz continuous function; thus, we apply spectral normalization [35] with a Lipschitz constant of 3. We use Xavier initialization [41] for each convolutional layer and uniform initialization for each linear layer (with mean 0 and variance 0.0001 for the weights). The bias of each layer is initialized with constant 0s.